Finite element analysis of unfastened cold-formed steel channel sections with web holes under end-two-flange loading at elevated temperatures

Kumar, Ankur; Roy, Krishanu; Uzzaman, Asraf; Lim, James B.P.

Published in:
Advanced Steel Construction

DOI:
10.18057/IJASC.2021.17.3.2

Published: 30/09/2021

FINITE ELEMENT ANALYSIS OF UNFASTENED COLD-FORMED STEEL CHANNELS WITH WEB HOLES UNDER END-TWO-FLANGE LOADING AT ELEVATED TEMPERATURES

Ankur Kumar[a], Krishanu Roy[b*], Asraf Uzzaman[c], James B.P. Lim[b]

[a] Department of Mechanical Engineering, Indian Institute of Technology Delhi, India

[b] Department of Civil and Environmental Engineering, The University of Auckland, New Zealand

[c] School of Computing, Engineering and Physical Sciences, University of the West of Scotland, Paisley, PA1 2BE, United Kingdom

Corresponding author: Krishanu Roy (kroy405@aucklanduni.ac.nz)

ABSTRACT

The paper presents a finite element analysis of G250 cold-formed steel (CFS) channel sections under end-two-flange (ETF) loading condition with circular web holes centred to load bearing plates and subjected to elevated temperatures. The stress strain curve for G250 CFS with 1.95 mm thickness at elevated temperatures was taken from Kankanamge and Mahendran and considered temperatures up to 700 °C. To analyse the effect of web hole size and bearing length on the strength of such sections at elevated temperatures, a parametric study involving a total of 288 FE models was performed. The parametric study results were used to assess the applicability of strength reduction factor equation presented by Uzzaman et al. for CFS C sections with web holes under ETF loading from ambient temperature to elevated temperatures. It was shown that the reduction factor equation is safe and reliable at elevated temperatures.

Keywords: CFS; Channel sections; End-Two-Flange; Web crippling; FEA; Elevated temperatures; Web holes.

1. INTRODUCTION

Cold-formed steel (CFS) is used increasingly in commercial and residential buildings because of its superior strength to weight ratio and stiffness, ease of construction and installation of sectional profiles [1-4]. These sections are usually provided with web holes in order to provide ease of electrical installation and plumbing services.

Web crippling is a well-known problem associated with such members, particularly when these are subjected to concentrated load near the web holes. This problem is exacerbated when such sections are subjected to elevated temperatures.

Significant published research is available on design guidance for CFS Channel(C) sections at ambient temperature under web crippling [5-10]. However, limited research is available on the effect that web holes have on the strength of C sections subject to concentrated load near the holes and under elevated temperatures. This lack of design information for CFS channels at elevated temperatures makes it difficult for practising engineers and researchers to predict the design capacity of CFS C sections under elevated temperatures and subject to web crippling.

Recent research has begun to focus upon the material behaviour of CFS sections at elevated temperature. Imran et al. [11] recently proposed numerical equations to evaluate the mechanical property reduction factors of square, rectangular and circular CFS hollow sections at elevated temperatures. Coupons were cut from such hollow sections and underwent temperatures ranging from 20^{o} C to 800^{o} C under steady state. The aim was to determine the reduction in material properties. Kankanamge and Mahendran [12] provided updated equations to predict material property reduction factors and the stress-strain relationship of low and high strength steel of different grades and thicknesses at elevated temperatures. A similar study was completed by Ranawaka and Mahendran [13], who proposed empirical equations in order to determine the stress-strain relationship of both high and low strength steel with multiple thickness values at elevated temperatures. Chen and Young [14] provided mechanical properties data for CFS grade of G550 and G450 by conducting tensile coupon tests under both steady and transient temperature conditions. Lim and Young [15] used the stress-strain relationship determined by the equations proposed by Chen and Young [14] to determine the effect of elevated temperatures on CFS bolted connections.

Alongside understanding change in mechanical properties of CFS sections at elevated temperatures, researchers are also focussing on understanding the structural behaviour of different CFS sections at elevated temperatures and subject to different loading conditions. Multiple investigations have been completed to determine the effect of elevated temperatures on CFS beams. Landesmann and Camotim [16] presented an FE investigation on the distortional post-buckling behaviour of CFS single-span lipped C beams under elevated temperatures. Laim et al. [17] completed the study so to understand the structural behaviour of CFS beams in fire. Kankanamge and Mahendran [18] presented a study using a validated FE model to determine the structural behaviour of CFS lipped C beams under bending at elevated temperatures.

Multiple studies have also been completed to understand the behaviour of CFS columns at elevated temperatures. Gunalan et al. [19] studied the local buckling behaviour of CFS lipped and unlipped C columns under simulated fire. Gunalan et al. [19] also presented a study on flexural-torsional buckling interaction of CFS lipped C columns at ambient and elevated temperatures. Ranawaka and Mahendran [20] have presented a study to determine the distortional buckling of CFS lipped C columns at elevated temperatures. Chen and Young [14] conducted a study using FEA to understand the behaviour of CFS lipped C columns at elevated temperatures. Feng and Wang [21] presented a study to evaluate the axial strength of CFS C columns under ambient and elevated temperatures.

It is to be noted that most of the research available in the current literature focuses on CFS sections under compression and torsional loading, and subject to fire boundary conditions. Almost nill focussed on the effect of web holes on the strength of CFS C sections when subject to web crippling at elevated temperature. Furthermore, current design specifications such as ASCE [22], EC3 [23] and BS5950 [24] does not provide any guidelines for CFS C sections with web holes at elevated temperatures under web crippling. This issue is addressed in the present paper.

Figure 1 shows symbol definitions used for the dimensions of the CFS C sections considered in this study. AS/NZ:4600 [25] offers reduction factor equations for CFS C sections with web holes. However, these are focussed on channels with web holes offset to the bearing edge and applicable only at normal temperature.

Goal of the paper is to determine the feasibility of design equations proposed in the literature for CFS C sections with web holes at ambient and elevated temperatures. In the literature, strength reduction factors have been given by Uzzaman et al. [26] for determining the centred web holes on unfastened CFS C sections subject to ETF loading at ambient temperature:

$$R = 0.90 + 0.12(N/h) - 0.60(a/h) \leq 1 \qquad \text{Equation (1)}$$

The limits for equation 1 are: $h/t \leq 156$, $N/h \leq 0.63$, $a/h \leq 0.8$, $N/t \leq 84$ and $\theta = 90^0$. Where, h is the depth of web's flat portion, t is thickness, N is the bearing length, and a is web hole diameter.

Equation (1), however, is applicable at ambient temperature and there is no information available for elevated temperatures. This paper considers if the same reduction factor equation is applicable to G250 CFS C sections subjected to ETF-loading at elevated temperatures. Kankanamge and Mahendran [12] provided stress-strain curves of G250 CFS with 1.95 mm thickness at elevated temperatures (Figure 2). These stress-strain curves are adopted in the present paper.

2. EXPERIMENTAL INVESTIGATION

Uzzaman et al. [27] conducted 44 experimental tests on CFS lipped C sections with web holes under ETF loading (Figure 3). Web hole size was varied so to determine its effect on web crippling strength of the C sections. The specimens were taken with centred web holes offset to bearing plates. Five different specimens were used with varying parameters such as nominal thickness, web depth, flange width, and web slenderness (h/t). To validate the developed non-linear FE model (details are given in Uzzaman et al. [27]), laboratory test results were used. The validated FE model was then incorporated to determine the strength reduction equation of such C sections with web holes and subject to ETF loading under web crippling. The detailed study can be found in Uzzaman et al. [27].

3. NUMERICAL INVESTIGATION

3.1 General

The present study developed the non-linear elastoplastic FE model using ANSYS [28] to investigate the web crippling behaviour of CFS C sections with web holes under elevated temperature. The main modelled components included: the bearing plates, C sections with and without web holes and the interface between the lipped C section and bearing plates. Details of the FE model in ANSYS [28] are summarised in the following sections.

3.2 Specimen Labelling

The modelled CFS C section dimensions are presented in Table 1. Figure 1 presents the symbol definitions used for the dimensions of the CFS C sections considered in the FE parametric study. The models have been coded so that condition of loading, specimen dimensions, bearing length as well as (a/h) ratio can be determined by the specimen label. For example, the label "ETF100 x 40 x 15 x 5 t-1.95 N50" is understood as outlined below. The first notation 'ETF' indicates the loading condition which is End-Two flange. The next three notations define the nominal dimension of the channel: '100 x 40 x 15' indicates the nominal depth, flange width and overall lip width of the section in millimetres; 't-1.95' indicates the thickness of the C section; and 'N50' shows the bearing length (i.e 50mm). The notation 'A0.4' indicates the value of (a/h) ratio and is 0.4. 'A0' denotes the C sections without web holes. Only unfastened flanges were considered in this study.

3.3 Mesh Sensitivity and Element Type

Figure 4 presents the FE mesh of CFS C section and the bearing plate. As the number of elements in the FE mesh increases, the accuracy of the results increases, as does computation time. In order to obtain acceptable results in a small amount of computation time, mesh size is varied. For the parametric study, the chosen mesh size of finite elements ranged from 3mm x 3mm (width by length) to 5mm x 5mm.

It is important to use finer meshing at the corners of C section because when the channel is subjected to loading, stresses are transferred from flange to web through these corners. The number of FE elements in the corner between web and flange was chosen at a value of 9. This value is maintained at 3 in the corners between the lip of the section and flange. Number of elements were decided so that the aspect ratio remained near to one. The region near the web holes was finely meshed. To optimise the mesh size and its numbers, mesh sensitivity analysis was performed.

Four-noded shell element SHELL 181 as given in the ANSYS library [28] was used to model the CFS C sections. Eight-noded solid element SOLID45 as given in ANSYS library [29] was used to model bearing plates. In order to model the surface interface between flanges and load bearing plates, CONTAT173 and TARGET170 elements were used.

3.4 Material and Geometry Properties

The FE model was the imitation of the test setup as presented in Uzzaman et al. [27] (Figure 3). The stress-strain curves of 1.95mm thick G250 CFS at elevated and normal temperatures were taken from Kankanamge and Mahendran [12] (Figure 2) and used to model the material in FEA programme. The considered material properties are summarised in Table 2. Equations 2 and 3 were incorporated to convert the engineering stress-strain relationship to the true stress-strain relationship as described in ANSYS manual [28].

$$\sigma_{true} = \sigma_{eng}(\varepsilon_{eng} + 1) \quad \text{(Equation 2)}$$

$$\varepsilon_{true} = \ln(\varepsilon_{eng} + 1) \quad \text{(Equation 3)}$$

3.5 Loading and Boundary Condition

The surface interaction was modelled between the load bearing plates and the flanges of C sections using the surface contact option in the ANSYS interaction library [28]. The two contact surfaces were constrained so not to penetrate one another. The displacement control method was used to model the vertical load applied to C section. Under this method, the nodes of the top bearing plate were displaced vertically to the predetermined value. In order to achieve the displacement of nodes of the top bearing plate only in y direction, all other degrees of freedom were constrained.

3.6 Verification of FE Model

For verification of the FE model, the results of FE analysis of CFS lipped C sections with centred web holes and subjected to ETF loading are presented in Table 3. The ratio of load per web determined by FEA and experiment shows good agreement was achieved between the experimental and FEA results. In order to provide the load displacement comparison between FEA and experimental results, the load displacement curve of specimen ETF142x60x13t-1.3N120 with a/h ratio ranging from 0 to 0.4 generated by FEA analysis is compared with the load displacement curve of same specimen obtained by experimental study (Figure 5). The comparison shows the validity of the FEA model.

4. Parametric Study

In this study, 288 FE analyses of CFS C sections with or without web holes with varying parameters such as sizes of web hole, bearing length and temperature ranging from 20 ^{0}C to 700 ^{0}C with an interval of 100 degrees were conducted. This study was completed to find out the effect of such parameters on the strength of CFS C sections with web hole at elevated temperatures subjected to web crippling.

Lian et al. [6-7] and Uzzaman et al. [26] have shown that the web crippling strength determined was influenced significantly by the a/h ratio, the N/h ratio. To determine the effect of a/h and N/h at different elevated temperatures on the web crippling strength of CFS C sections with web holes, a parametric study was completed to consider the different web hole sizes and bearing plate lengths. The specimens included three sections – C100, C125 and C150 with nominal depths of 100, 125 and 150 mm. Three different bearing plate lengths of 50mm, 75mm and 100mm were considered. The (a/h) ratio were 0, 0.4, 0.6 and 0.8. The inside corner radii between hole and web was 5mm. For every specimen, the web crippling strength at different N/h and a/h ratio at particular elevated temperature were obtained, as summarised in Tables 5(a), 5(b) and 5(c). Thus, the strength reduction factor

(R) at particular temperatures ranging from 20 degrees to 700 degrees as presented in Tables 5(a), 5(b) and 5(c) was incorporated to determine the deteriorating effect of the web holes on the web crippling strength. After obtaining the reduction factor values for every particular temperature, the reduction factor values were compared with the reduction factor values predicted using the equation presented in Uzzaman et al. [26] for web crippling of CFS C sections at ambient temperatures (see Tables 5(a), 5(b) and 5(c), Figures 7(a) and 7(b)).

Figure 6(a) presents the comparison of strength reduction factor a/h ratio. It is found that the strength reduction happens in proportion to the change in a/h for every specific temperature ranging from 20^0 C to 700^0 C.

Figure 6(b) presents the comparison of (N/h) ratio versus the strength reduction factor. It is found that the strength reduction was insensitive to the N/h ratio for temperatures ranging from 20^0 C to 700^0 C.

5. Reduction Factor Comparison

The reduction factor equation proposed by Uzzaman et al. [26] for CFS unfastened C sections with centred web hole under ETF loading is determined by equation (1). To determine the efficacy of the proposed equation to CFS at elevated temperature, numerical analysis was performed on the above equation. Tables 5(a), 5(b) and 5(c) (see Figures 7(a) and 7(b)) compares the reduction factors determined by the FE models in equation 1 for the case of unfastened C sections with centred web holes at elevated temperature.

In order to calculate the reliability index, a resistance factor (ϕ) of 0.90 was used. Load combination 1.2DL + 1.6 LL (DL = Dead load, LL = Live Load) as mentioned in NAS specification [28] was used. M_m = 1.10 (Mean) and V_m = 0.10 (Coefficient of variation) was used for the material properties, respectively. The mean value (F_m) and coefficient of variation (V_F) used in the reliability analysis were 1.00 and 0.05, respectively. As can be seen, for every specific temperature ranging from 20^0 to 700^0 C, the β (reliability factor) value was greater than 2.5 (see Table 6). For the parametric study, the reliability factor is. Greater than 2.5 (Figure 8). This is the target reliability index value for CFS structural members and is recommended as the lower limit under North American specification [29]. This shows that the proposed strength reduction factor equation by Uzzaman et al. [26] is effective in determining the effect of circular web hole on the web crippling strength of CFS at elevated temperatures.

6. Conclusion

A study has been completed to determine the influence of circular web hole and bearing length on the web crippling strength of G250 CFS channels when subjected to ETF loading at elevated temperatures. The parametric study comprising 288 FE analyses with varying dimensions and constant thickness was conducted. The study included cases with and without web holes.

To determine the efficacy of the strength reduction factor equation given by Uzzaman et al. [26] at elevated temperatures, the reduction factor equation given by Uzzaman et al. [26] for CFS channels subjected to ETF loading at ambient temperature was studied in order to find out its applicability to elevated temperatures. After statistical analysis in the form of reliability analysis, it was found that the equation proposed by Uzzaman et al. [26] is applicable to elevated temperatures. It was found that the strength reduction factor equation given by Uzzaman et al. [26] is capable to produce safe and reliable design values when a resistance factor of 0.90 (ϕ = 0.90) for CFS C section with web hole subjected to ETF loading under elevated temperatures was used. This also ensured that the design values were not too conservative.

REFERENCES

[1] Javed, F. M., Hafizah , N., Memon , A. S., Jameel , M., & Aslam , M. (2017). Recent research on cold formed steel beams and columns at elevated temperature: A review. Construction and Building Materials, 144, 686-701.

[2] Darcy, G., & Mahendran, M. (2008). Development of a new cold formed steel building system. Advances in Structural Engineering, 11(6), 661-677.

[3] Schafer, B. (2002). Local, distortional and euler buckling of thin-walled columns. Journal of Structural Engineering, 128(3), 289-299.

[4] Roy, K., Lim, J. B., Lau, H. H., Yong, P., Clifton, G., Johnston, R. P., . . . Mei, C. C. (2019). Collapse Behaviour of a Fire Engineering Designed Single-Storey Cold Formed Steel Building in Fires. Thin Walled structures, 142, 340-357.

[5] Uzzaman , A., Lim , J. B., Nash, D., Rhodes , J., & Young , B. (2013). Effect of offset web holes on web crippling strength cold-formed steel channel sections under end-two flange loading condition. Thin Walled Structures, 65, 34-48.

[6] Lian, Y., Uzzaman, A., Lim, J., Abdelal, G., Nash, D., & Young, B. (2017). Effect of Web holes on web crippling strength of cold formed steel channel sections under interior-one-flange loading condition - Part I: Tests and finite element analysis. Thin Walled Structures, 111, 103-12.

[7] Lian, Y., Uzzaman, A., Lim, J., Abdelal, G., Nash, D., & Young, B. (2017). Effect of Web holes on web crippling strength of cold formed steel channel sections under end-one-flange loading condition - Part II Parametric study and proposed design equation. Thin Walled Structures, 111, 103-12.

[8] Gunalan, S., Heva, Y. B., & Mahendran, M. (2015). Local buckling studies of cold formed steel compression members at elevated temperatures. Journal of Constructional Steel Research, 108, 31-45.

[9] Gunalan, S., Mahendran, M. (2019). Experimental study of unlipped channel beams subject to web crippling under one flange load case. Journal of Advanced Steel Construction, 15, 165-172

[10] Elilarasi, K., Kasturi, S., Janarthan, B. (2020). Effect of Circular openings on Web Crippling of Unlipped channel sections under End-two-flange load case. Journal of Advanced Steel Construction, 16, 310-320

[11] Imran, M., Mahendran, M., & Poologanathan, K. (2018). Mechanical properties of cold formed steel tubular sections at elevated temperatures. Journal of Constructional Steel Research, 143, 131-147.

[12] Kankanamge, N. D., & Mahendran, M. (2011). Mechanical properties of cold formed steel at elevated temperatures. Thin Walled Structures, 49, 26-44.

[13] Ranawaka, T., & Mahendran, M. (2009). Experimental study of the mechanical properties of light gauge cold formed steels at elevated temperatures. Fire Safety Journal, 44, 219-229.

[14] Chen, J., & Young, B. (2007). Experimental investigation of cold formed steel material at elevated temperatures. Thin Walled Structures, 45(1), 96-110.

[15] Lim, J., & Young, B. (2007). Effects of elevated temperatures on bolted moment connections between cold formed steel members. Engineering Structures, 29, 2419-2427.

[16] Landesmann, A., & Camotim, D. (2016). Distortional failure and DSM design of cold-formed steel lipped channel beams under elevated temperatures. Thin Walled Structures, 98, 75-93.

[17] Laim L. Rodrigues Joao Paulo C., Craveiro Helder D. (2016). Flexural behaviour of axially and rotationally re-strained cold-formed steel beams subjected to fire. Thin Walled Structures, 98, 39-47

[18] Kankanamge, N. D., & Mahendran M. (2012). Behavior and design of cold formed steel beams subjected to lateral torsional buckling at elevated temperatures. 61, 213-228.

[19] Gunalan, S., Heva, B. Y., & Mahendran, M. (2014). Flexural-Torsional buckling behaviour and design of cold formed steel compression members at elevated temperatures. Engineering Structures, 79, 149-168.

[20] Ranawaka, T., & Mahendran, M. (2010). Numerical modelling of light gauge cold formed steel compression members subjected to distortional buckling at elevated temperatures. Thin Walled Structures, 48, 334-344.

[21] Feng, M., & Wang, Y. (2003). Structural behaviour of cold-formed thin-walled short steel channel columns at elevated temperatures. Part I experiments. Thin-Walled Structures, 41, 543-570.

[22] ASCE. ((2005)). Minimum design loads for buildings and other structures. American Society of Civil Engineers Standard.

[23] BS EN 1993-1-1 Eurocode 3. Design of Steel Structures. General requirements, British Standards Institutions;2005

[24] BS5950 (1998). Structural use of steelwork in buildings. Part 5 Code of practice for the design of cold-formed sections, London: British Standard Institution

[25] AS/NZS Standards Australia. Cold Formed Steel Structures, AS/NZS 4600:2018, Standards Australia/Standards New Zealand, 2018

[26] Uzzaman, A., Lim, J., Nash, D., Rhodes, J., & Young, B. (2012). Cold-formed steel sections with web openings subjected to web crippling under two-flange loading

conditions - Part II: Parametric study and proposed design equations. Thin-Walled Structures, 56, 79-87.

[27] Uzzaman, A., Lim, J., Nash, D., Rhodes, J., & Young, B. (2012). Cold-formed steel sections with web openings subjected to web crippling under two-flange loading conditions - Part I: Tests and Finite element analysis. Thin-Walled Structures, 56, 38-48

[28] ANSYS. (2017). User's Manual, revision 17.0. Swanson Analysis System.

[29] NAS, North American Specification for the design of cold-formed steel structural members. AISI S100-2007, AISI Standard. American Iron and Steel Institute;2007.

List of Symbols	
a	Diameter of circular web hole;
a/h	Web hole ratio;
b_f	flange width;
b_l	lip width;
d	Depth of cross-section;
E	Young's modulus of elasticity;
FEA	Finite element analysis;
h	Depth of the web's flat portion;
L	Specimen length;
N	Bearing plate length;
N/h	Bearing length ratio;
P_{EXP}	Experimental ultimate web crippling load per web;
P_{FEA}	Web crippling strength per web predicted from FEA;
P_m	Mean;

r_q	Inside fillet radius between web and hole;
r_i	Inside fillet radius of section;
R_{FEA}	Reduction factor obtained from FEA study;
$R_{Uzzaman}$	Reduction factor obtained from Uzzaman et al. (2012);
t	Thickness of the section;
f_u f_y	Static ultimate tensile strength; Yield stress;
β	Reliability index;
V_p	Coefficient of variation;
ϕ	Resistance factor;
σ_{true}	True stress;
σ	Engineering stress;
ε	Engineering strain;
$\varepsilon_{true,pl}$	True plastic strain;

Table 1 Dimension of specimens considered in the study

Specimen	Web d(mm)	Flange b_f(mm)	Lip h_l(mm)	Length L(mm)	Thickness t(mm)	Fillet r_i(mm)	Web depth h(mm)	Web slenderness h/t	Bearing length N(mm)	Bearing Length ratio N/h	Web hole Ratio a/h	Diameter of web hole a(mm)
ETF100x40x15-t-1.95N50A0	100	40	15	350	1.95	5	98.1	50.3	50	0.51	0	0
ETF100x40x15t-1.95N50A0.4	100	40	15	350	1.95	5	98.1	50.3	50	0.51	0.4	39.22
ETF100x40x15-t-1.95N75A0	100	40	15	375	1.95	5	98.1	50.3	75	0.76	0	0
ETF100x40x15-t-1.95N75A0.4	100	40	15	375	1.95	5	98.1	50.3	75	0.76	0.4	39.22
ETF 125x40x15-t-1.95N50A0	125	40	15	425	1.95	5	123.1	63.1	50	0.41	0	0
ETF 125x40x15-t-1.95N50A0.4	125	40	15	425	1.95	5	123.1	63.1	50	0.41	0.4	49.22
ETF 125x40x15-t-1.95N50A0.6	125	40	15	425	1.95	5	123.1	63.1	50	0.41	0.6	73.83
ETF 125x40x15-t-1.95N50A0.8	125	40	15	425	1.95	5	123.1	63.1	50	0.41	0.8	98.44
ETF 125x40x15-t-1.95N75A0	125	40	15	450	1.95	5	123.1	63.1	75	0.61	0	0
ETF 125x40x15-t-1.95N75A0.4	125	40	15	450	1.95	5	123.1	63.1	75	0.61	0.4	49.22
ETF 125x40x15-t-1.95N75A0.6	125	40	15	450	1.95	5	123.1	63.1	75	0.61	0.6	73.83
ETF 125x40x15-t-1.95N75A0.8	125	40	15	450	1.95	5	123.1	63.1	75	0.61	0.8	98.44
ETF 125x40x15-t-1.95N100A0	125	40	15	475	1.95	5	123.1	63.1	100	0.81	0	0
ETF 125x40x15-t1.95N100A0.4	125	40	15	475	1.95	5	123.1	63.1	100	0.81	0.4	49.22
ETF 125x40x15-t1.95N100A0.6	125	40	15	475	1.95	5	123.1	63.1	100	0.81	0.6	73.83
ETF 125x40x15-t1.95N100A0.8	125	40	15	475	1.95	5	123.1	63.1	100	0.81	0.8	98.44
ETF 150x40x15-t-1.95N50A0	150	40	15	500	1.95	5	148.1	75.9	50	0.34	0	0
ETF 150x40x15-t-1.95N50A0.4	150	40	15	500	1.95	5	148.1	75.9	50	0.34	0.4	59.22
ETF 150x40x15-t-1.95N50A0.6	150	40	15	500	1.95	5	148.1	75.9	50	0.34	0.6	88.83
ETF 150x40x15-t-1.95N50A0.8	150	40	15	500	1.95	5	148.1	75.9	50	0.34	0.8	118.44
ETF 150x40x15-t-1.95N75A0	150	40	15	525	1.95	5	148.1	75.9	75	0.51	0	0
ETF 150x40x15-t-1.95N75A0.4	150	40	15	525	1.95	5	148.1	75.9	75	0.51	0.4	59.22
ETF 150x40x15-t-1.95N75A0.6	150	40	15	525	1.95	5	148.1	75.9	75	0.51	0.6	88.83
ETF 150x40x15-t-1.95N75A0.8	150	40	15	525	1.95	5	148.1	75.9	75	0.51	0.8	118.44
ETF 150x40x15-t-1.95N100A0	150	40	15	550	1.95	5	148.1	75.9	100	0.68	0	0
ETF 150x40x15-t1.95N100A0.4	150	40	15	550	1.95	5	148.1	75.9	100	0.68	0.4	59.22
ETF 150x40x15-t1.95N100A0.6	150	40	15	550	1.95	5	148.1	75.9	100	0.68	0.6	88.83
ETF 150x40x15-t1.95N100A0.8	150	40	15	550	1.95	5	148.1	75.9	100	0.68	0.8	118.44

Table 2 Material properties of G250 CFS of 1.95 mm thickness (Kankanamge and Mahendran [12])

Temp (°C)	σu (T) (MPa)	E(Mpa)	fy(Mpa)
20	356.1	188220	270.5
100	369.0	179640	267.3
200	435.2	171745	257.0
300	385.0	154330	196.4
400	240.0	121230	147.7
500	137.5	90631	95.8
600	71.4	57777	54.1
700	37.7	31363	34.4

TABLE 3 Comparison of finite element analysis with the experiment results for flanges unfastened under ETF loading condition

Specimen	Web d (mm)	Flange b_f (mm)	Lip b_l (mm)	Thickness t (mm)	Fillet r_i (mm)	Holes a (mm)	Length L (mm)	Exp. load per web P_{EXP} (kN)	Web Crippling Strength per web predicted from P_{FEA} (kN)	Comparison P_{EXP}/P_{FEA}
ETF142x60x13-t1.3N90A0	142.2	58.6	15.9	1.23	4.8	0.0	337.5	2.21	2.18	1.01
ETF142x60x13-t1.3N90A0.2	142.2	58.6	15.9	1.23	4.8	27.9	337.5	1.98	1.94	1.02
ETF142x60x13-t1.3N90A0.4	142.2	59.5	16.3	1.25	4.8	55.8	337.5	1.62	1.69	0.96
ETF142x60x13-t1.3N90A0.6	142.2	59.5	16.3	1.25	4.8	83.6	337.5	1.32	1.41	0.94
ETF172x65x13-t1.3N120A0	172.8	64.1	15.6	1.27	5.0	0.0	400.0	2.37	2.28	1.04
ETF172x65x13-t1.3N120A0.4	172.3	63.6	15.5	1.27	5.0	67.6	400.0	1.70	1.81	0.94
ETF172x65x13-t1.3N120A0.6	172.6	64.3	15.3	1.28	5.0	101.6	400.0	1.36	1.48	0.92
ETF202x65x13-t1.4N120A0	202.1	63.1	17.5	1.45	5.0	0.0	425.0	2.70	2.87	0.94
ETF202x65x13-t1.4N120A0.2	202.7	64.3	16.3	1.45	5.0	39.8	425.0	2.41	2.46	0.98
ETF202x65x13-t1.4N120A0.4	202.4	64.2	16.5	1.45	5.0	79.5	425.0	1.88	2.01	0.94
ETF202x65x13-t1.4N150A0	202.1	63.1	17.5	1.45	5.0	0.0	450.0	2.84	3.29	0.86
ETF202x65x13-t1.4N150A0.4	202.7	64.3	16.3	1.45	5.0	79.5	450.0	2.19	2.35	0.93
ETF202x65x13-t1.4N150A0.6	202.4	64.2	16.5	1.45	5.0	119.5	450.0	1.77	1.90	0.93

Table 4 Parametric study of web crippling strength at elevated temperatures

4(a) ETF100x45x15-t1.95

			FEA Load per Web (kN) at (a/h)			
Temperature(°C)	N(mm)	N/h	A0	A0.4	A0.6	A0.8
20			4.12	3.13	2.66	2.24
100			3.84	3.02	2.60	2.22
200			4.35	3.33	2.87	2.43
300	50	0.51	3.23	2.50	2.15	1.82
400			2.61	2.02	1.74	1.47
500			1.85	1.43	1.23	1.04
600			1.13	0.87	0.75	0.64
700			0.62	0.48	0.41	0.35
20			4.97	3.85	3.35	2.88
100			4.60	3.68	3.23	2.79
200			5.25	4.08	3.57	3.10
300			3.90	3.07	2.68	2.32
400	75	0.76	3.14	2.48	2.16	1.87
500			2.21	1.74	1.53	1.32
600			1.34	1.06	0.93	0.81
700			0.74	0.58	0.51	0.44
20			5.82	4.62	4.09	3.56
100			5.35	4.37	3.88	3.38
200			6.16	4.90	4.32	3.77
300			4.59	3.69	3.25	2.83
400	100	1.02	3.68	2.96	2.62	2.28
500			2.57	2.07	1.84	1.61
600			1.56	1.25	1.12	0.98
700			0.87	0.69	0.62	0.54

4(b) ETF125x45x15-t1.95

			FEA Load per Web (kN) at (a/h)			
Temperature(°C)	N(mm)	N/h	A0	A0.4	A0.6	A0.8
20			3.80	2.85	2.38	1.94
100			3.63	2.77	2.34	1.93
200			4.08	3.02	2.54	2.07
300			2.98	2.23	1.87	1.53
400	50	0.41	2.43	1.83	1.54	1.26
500			1.76	1.32	1.12	0.92
600			1.08	0.81	0.69	0.56
700			0.59	0.44	0.37	0.30
20			4.49	3.41	2.91	2.46
100			4.26	3.29	2.83	2.42
200			4.83	3.61	3.08	2.62
300			3.54	2.67	2.28	1.93
400	75	0.61	2.87	2.18	1.87	1.59
500			2.06	1.57	1.36	1.15
600			1.27	0.96	0.83	0.71
700			0.69	0.52	0.45	0.38
20			5.21	4.02	3.48	2.99
100			4.92	3.85	3.35	2.89
200			5.63	4.27	3.68	3.16
300			4.14	3.16	2.72	2.33
400	100	0.81	3.34	2.57	2.22	1.91
500			2.38	1.85	1.61	1.39
600			1.46	1.13	0.99	0.85
700			0.80	0.62	0.53	0.46

4(c) ETF150x45x15-t1.95

			FEA Load per Web (kN) at (a/h)			
Temperature(°C)	N(mm)	N/h	A0	A0.4	A0.6	A0.8
20			3.53	2.62	2.16	1.72
100			3.45	2.56	2.13	1.71
200			3.83	2.76	2.28	1.81
300			2.77	2.01	1.66	1.32
400	50	0.34	2.28	1.67	1.38	1.10
500			1.67	1.23	1.03	0.82
600			1.04	0.76	0.63	0.50
700			0.56	0.41	0.34	0.27
20			4.09	3.07	2.58	2.14
100			3.98	2.99	2.53	2.11
200			4.45	3.24	2.71	2.24
300			3.23	2.37	1.98	1.64
400	75	0.51	2.65	1.96	1.64	1.36
500			1.93	1.44	1.22	1.01
600			1.20	0.89	0.75	0.62
700			0.64	0.48	0.40	0.33
20			4.69	3.56	3.02	2.56
100			4.56	3.45	2.95	2.51
200			5.13	3.76	3.19	2.68
300			3.73	2.76	2.33	1.96
400	100	0.68	3.05	2.27	1.93	1.63
500			2.21	1.66	1.42	1.21
600			1.37	1.02	0.88	0.74
700			0.74	0.55	0.47	0.40

Table 5 Comparison of web crippling strength reduction factor with reduction factor equation proposed by Uzzaman et al. [26]

5(a) ETF-100x45x15-t1.95

			Reduction Factor			Comparison with resistance from Uzzaman et al. [26] ($R/R_{Uzzaman}$)		
Temperature(°C)	N(mm)	N/h	R = P(A0.4)/P(A0)	R = P(A0.6)/P(A0)	R = P(A0.8)/P(A0)	A0.4	A0.6	A0.8
20			0.76	0.65	0.54	1.05	1.07	1.13
100			0.79	0.68	0.58	1.09	1.13	1.20
200			0.77	0.66	0.56	1.06	1.10	1.16
300			0.77	0.67	0.57	1.07	1.11	1.17
400	50	0.51	0.78	0.67	0.56	1.08	1.11	1.17
500			0.77	0.67	0.57	1.07	1.11	1.18
600			0.77	0.66	0.56	1.07	1.10	1.17
700			0.77	0.66	0.56	1.07	1.10	1.16
20			0.78	0.68	0.58	1.03	1.07	1.13
100			0.80	0.70	0.61	1.07	1.11	1.19
200			0.78	0.68	0.59	1.04	1.08	1.16
300			0.79	0.69	0.59	1.05	1.09	1.16
400	75	0.76	0.79	0.69	0.60	1.05	1.09	1.17
500			0.79	0.69	0.60	1.05	1.10	1.17
600			0.79	0.69	0.60	1.05	1.10	1.18
700			0.79	0.69	0.60	1.05	1.09	1.16
20			0.79	0.70	0.61	1.02	1.06	1.13
100			0.82	0.72	0.63	1.04	1.09	1.16
200			0.80	0.70	0.61	1.02	1.06	1.13
300			0.80	0.71	0.62	1.03	1.07	1.13
400	100	1.02	0.81	0.71	0.62	1.03	1.07	1.14
500			0.81	0.72	0.63	1.03	1.08	1.16
600			0.80	0.72	0.63	1.03	1.08	1.16
700			0.80	0.71	0.62	1.02	1.07	1.15

5(b) ETF125x45x15t1.95

			Reduction Factor			Comparison with resistance from Uzzaman et al. [26] ($R/R_{Uzzaman}$)		
Temperature(°C)	N(mm)	N/h	R = P(A0.4)/P(A0)	R = P(A0.6)/P(A0)	R = P(A0.8)/P(A0)	A0.4	A0.6	A0.8
20			0.75	0.63	0.51	1.06	1.06	1.09
100			0.76	0.65	0.53	1.08	1.10	1.14
200			0.74	0.62	0.51	1.04	1.05	1.08
300			0.75	0.63	0.51	1.05	1.06	1.10
400	50	0.41	0.75	0.63	0.52	1.06	1.07	1.10
500			0.75	0.64	0.52	1.06	1.08	1.11
600			0.75	0.63	0.52	1.06	1.08	1.10
700			0.75	0.63	0.51	1.05	1.07	1.09
20			0.76	0.65	0.55	1.03	1.05	1.11
100			0.77	0.67	0.57	1.05	1.08	1.15
200			0.75	0.64	0.54	1.02	1.04	1.10
300			0.75	0.64	0.55	1.03	1.05	1.11
400	75	0.61	0.76	0.65	0.55	1.04	1.06	1.12
500			0.76	0.66	0.56	1.04	1.07	1.13
600			0.76	0.66	0.56	1.04	1.07	1.13
700			0.76	0.65	0.55	1.03	1.06	1.12
20			0.77	0.67	0.57	1.02	1.05	1.11
100			0.78	0.68	0.59	1.03	1.07	1.14
200			0.76	0.65	0.56	1.00	1.03	1.09
300			0.76	0.66	0.56	1.01	1.03	1.09
400	100	0.81	0.77	0.67	0.57	1.02	1.05	1.11
500			0.77	0.67	0.58	1.02	1.06	1.13
600			0.77	0.67	0.58	1.02	1.06	1.13
700			0.77	0.67	0.57	1.01	1.05	1.11

5(c) ETF150x45x15t1.95

Temperature(°C)	N(mm)	N/h	Reduction Factor R = P(A0.4)/P(A0)	Reduction Factor R = P(A0.6)/P(A0)	Reduction Factor R = P(A0.8)/P(A0)	Comparison with resistance from Uzzaman et al. [26] ($R/R_{Uzzaman}$) A0.4	A0.6	A0.8
20			0.74	0.61	0.49	1.06	1.06	1.06
100			0.74	0.62	0.50	1.06	1.07	1.08
200			0.72	0.59	0.47	1.03	1.02	1.03
300			0.73	0.60	0.48	1.04	1.03	1.04
400	50	0.34	0.73	0.61	0.48	1.05	1.04	1.05
500			0.74	0.61	0.49	1.05	1.05	1.06
600			0.73	0.61	0.48	1.05	1.05	1.05
700			0.73	0.60	0.48	1.04	1.04	1.04
20			0.75	0.63	0.52	1.04	1.05	1.08
100			0.75	0.63	0.53	1.04	1.06	1.10
200			0.73	0.61	0.50	1.01	1.01	1.05
300			0.73	0.61	0.51	1.02	1.02	1.05
400	75	0.51	0.74	0.62	0.51	1.03	1.03	1.07
500			0.74	0.63	0.52	1.03	1.05	1.09
600			0.74	0.63	0.52	1.03	1.04	1.08
700			0.74	0.62	0.51	1.02	1.03	1.07
20			0.76	0.64	0.55	1.02	1.04	1.09
100			0.76	0.65	0.55	1.02	1.04	1.10
200			0.73	0.62	0.52	0.99	1.00	1.04
300			0.74	0.62	0.53	1.00	1.00	1.05
400	100	0.68	0.75	0.63	0.53	1.01	1.02	1.07
500			0.75	0.64	0.55	1.01	1.03	1.09
600			0.75	0.64	0.54	1.01	1.03	1.08
700			0.75	0.63	0.54	1.00	1.02	1.07

Table 6 Statistical analysis for determining the applicability of strength reduction factor proposed by Uzzaman et al. [26] for ETF loading at ambient temperature to elevated temperature.

	Statistical Parameters R_{FEA}/R_p ((0.90 – 0.60(a/h) + 0.12(N/h))			
Temperature(^{0}C)	Mean, P_m	Coefficient of Variation V_p	Reliability index β	Resistance Factor ϕ
20	1.07	0.03	2.85	0.90
100	1.09	0.04	2.93	0.90
200	1.05	0.04	2.77	0.90
300	1.06	0.04	2.81	0.90
400	1.07	0.04	2.85	0.90
500	1.08	0.04	2.88	0.90
600	1.07	0.04	2.86	0.90
700	1.07	0.04	2.83	0.90

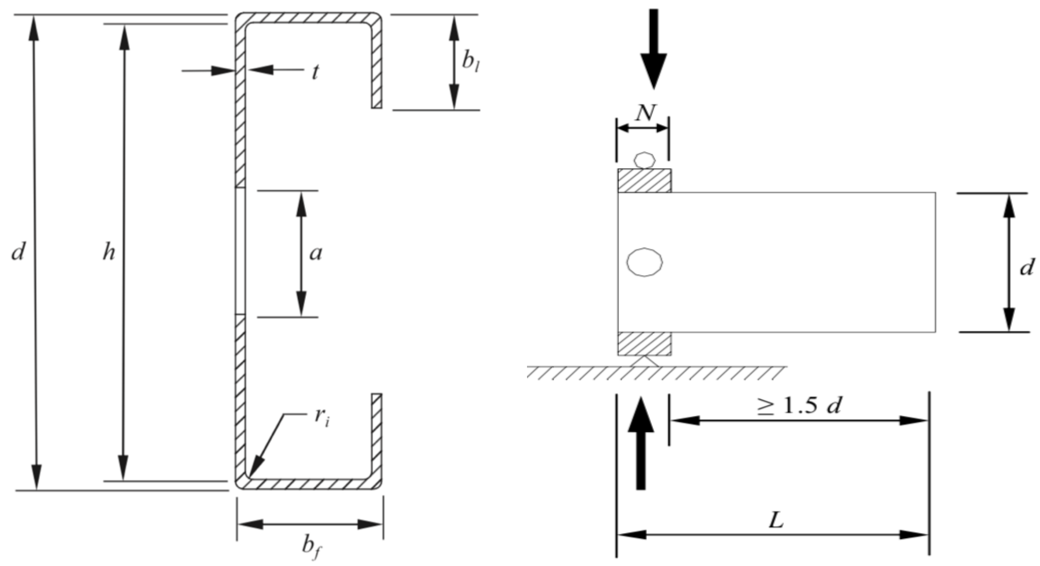

Figure 1 Definition of symbols

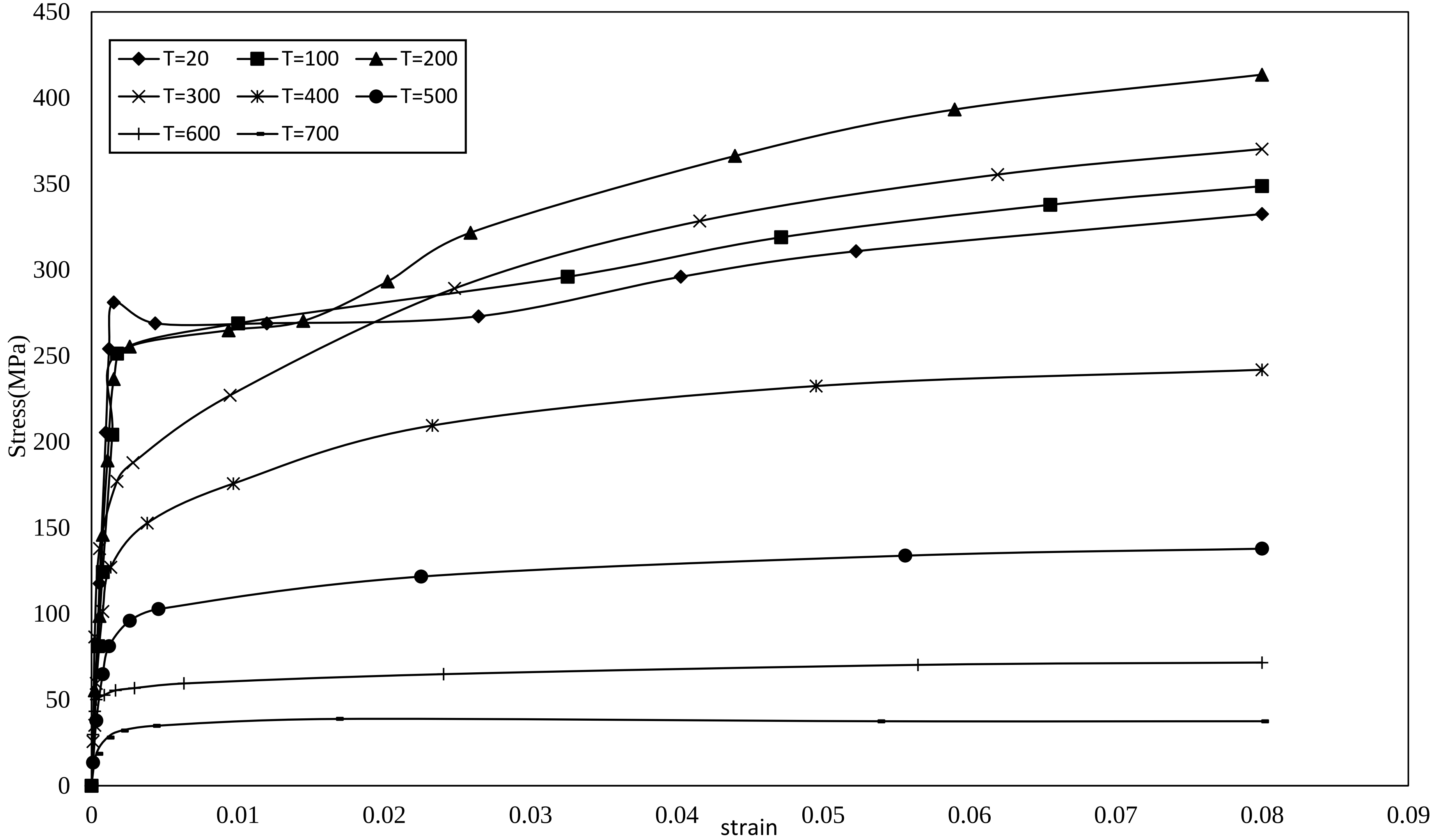

Figure 2 Stress Strain curves (Kankanamge and Mahendran [12])


a)


b)

Figure 3 Experimental analysis of CFS lipped C sections (unfastened flanges) under ETF loading condition after Uzzaman et al. [26]: a) centred circular web hole and b) offset circular web hole

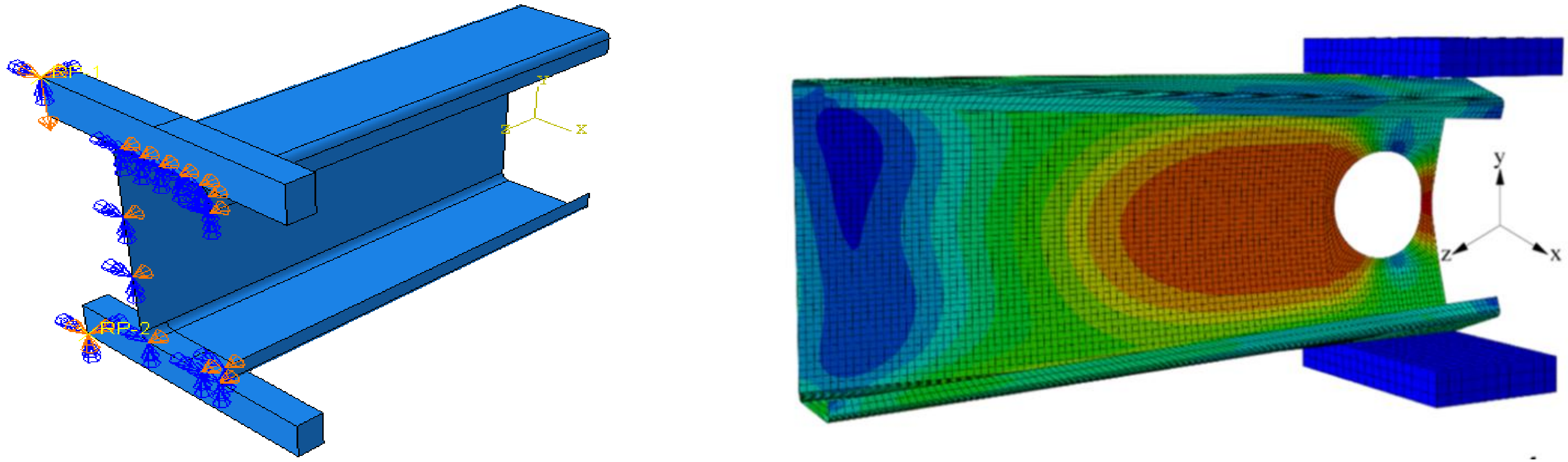

Figure 4 a) Boundary conditions applied in FEA model for ETF-100x45x15-t1.95N50A0 b) Deformed shape predicted by FEA model for ETF-125x45x15t1.95N100A0.4

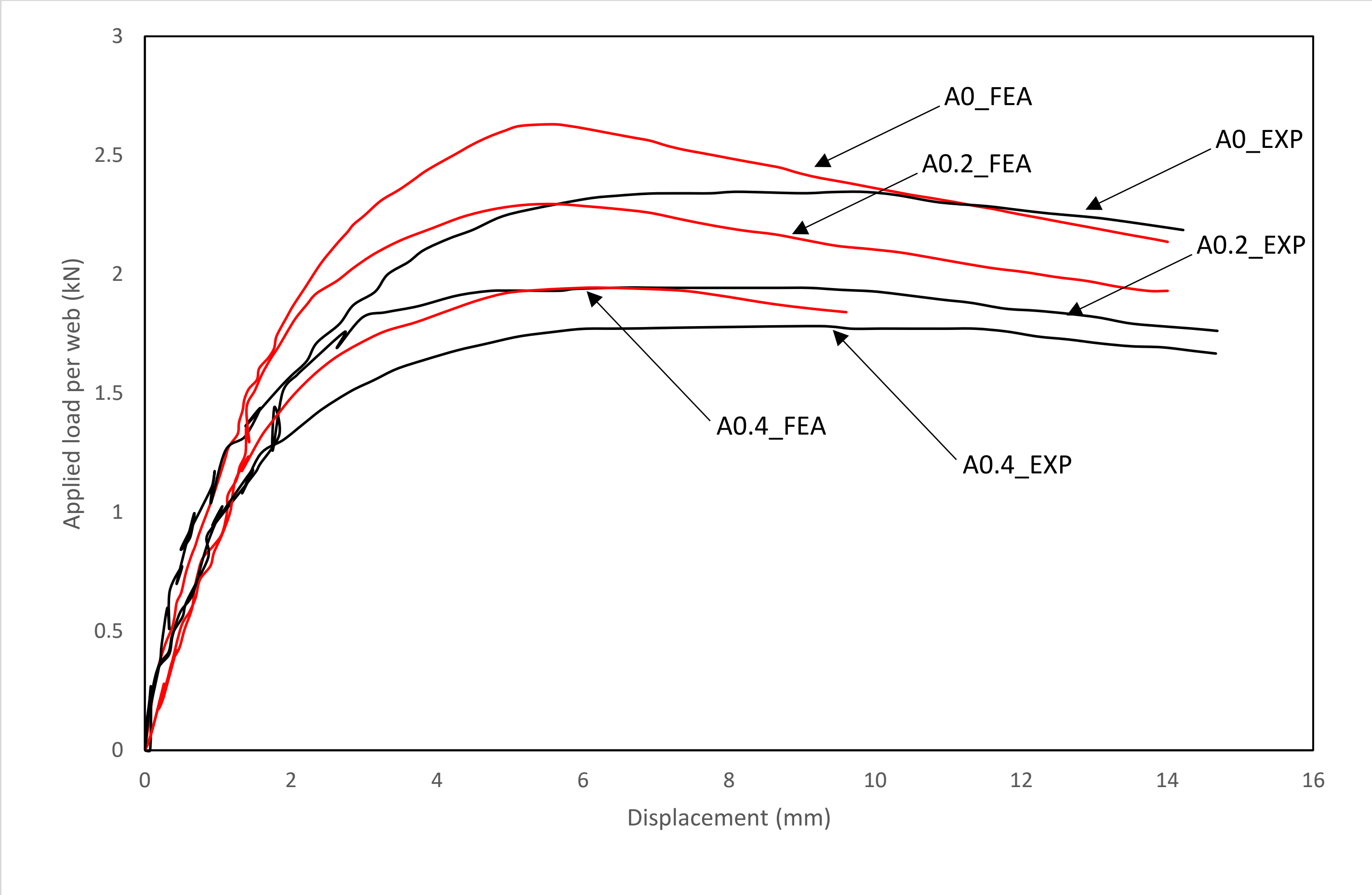

Figure 5 Comparison of web deformation curves for specimen ETF142x60x13t-13N120

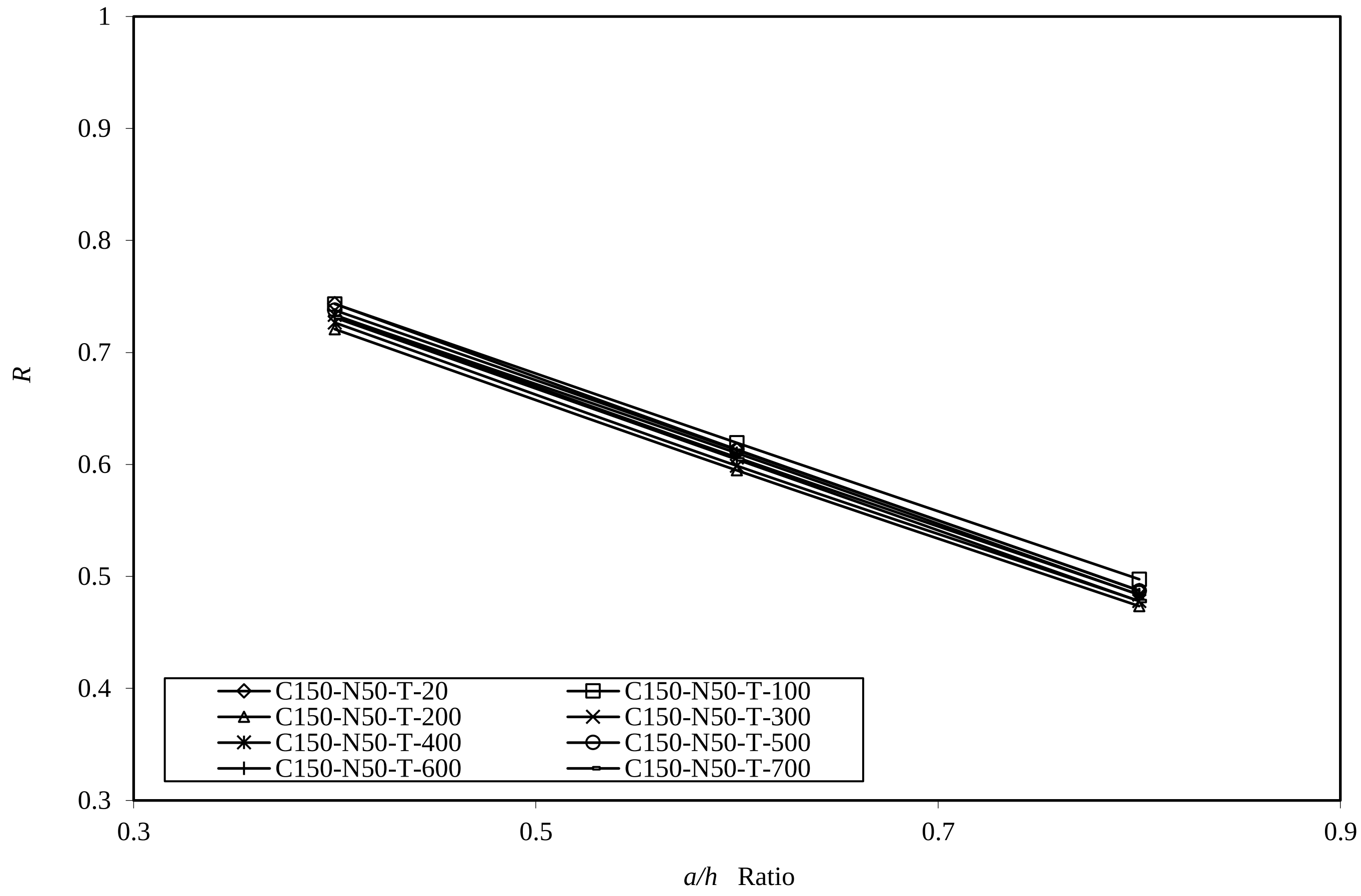

1
0.9
0.8
0.7
0.6
0.5
0.4
0.3
R
0.3
0.5
0.7
0.9
a/h Ratio
C150-N50-T-20
C150-N50-T-100
C150-N50-T-200
C150-N50-T-300
C150-N50-T-400
C150-N50-T-500
C150-N50-T-600
C150-N50-T-700

(a)

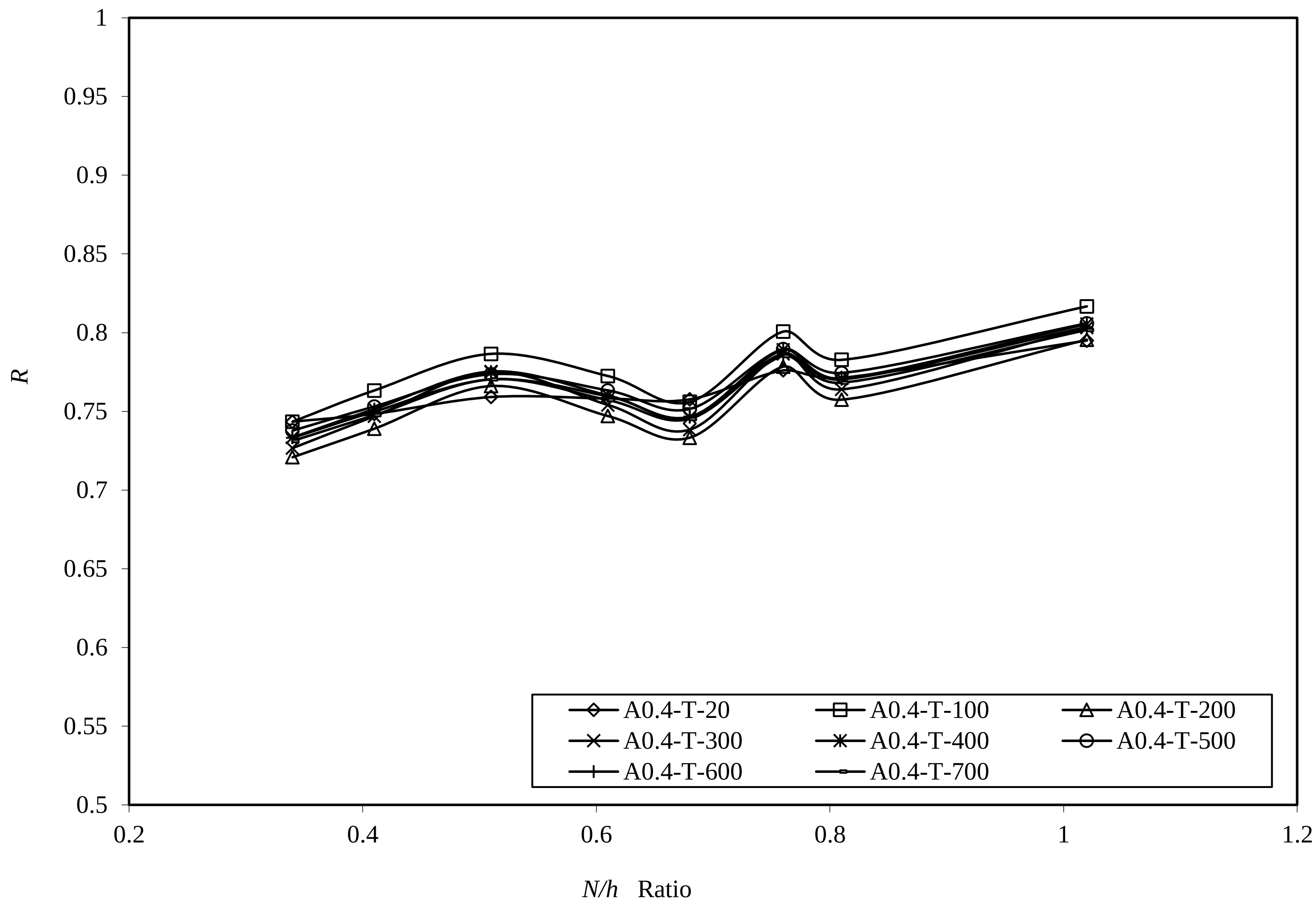

(b)

Figure 6 Variation in reduction factors : a) with a/h ratio, b) with N/h ratio.

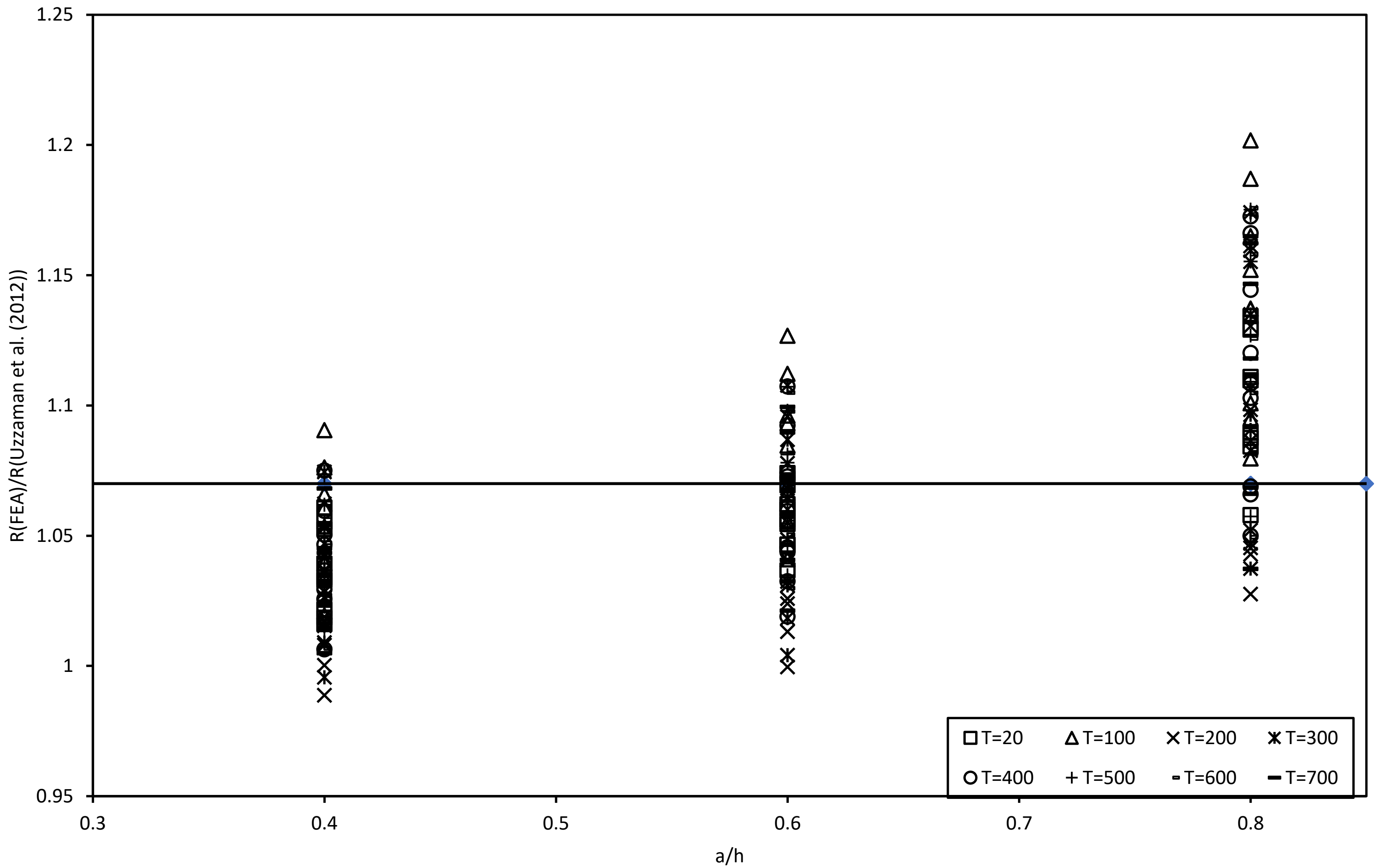

1.25
1.2
1.15
1.1
1.05
1
0.95
R(FEA)/R(Uzzaman et al. (2012))
0.3
0.4
0.5
0.6
0.7
0.8
a/h
T=20
T=100
T=200
T=300
T=400
T=500
T=600
T=700

S

(a)

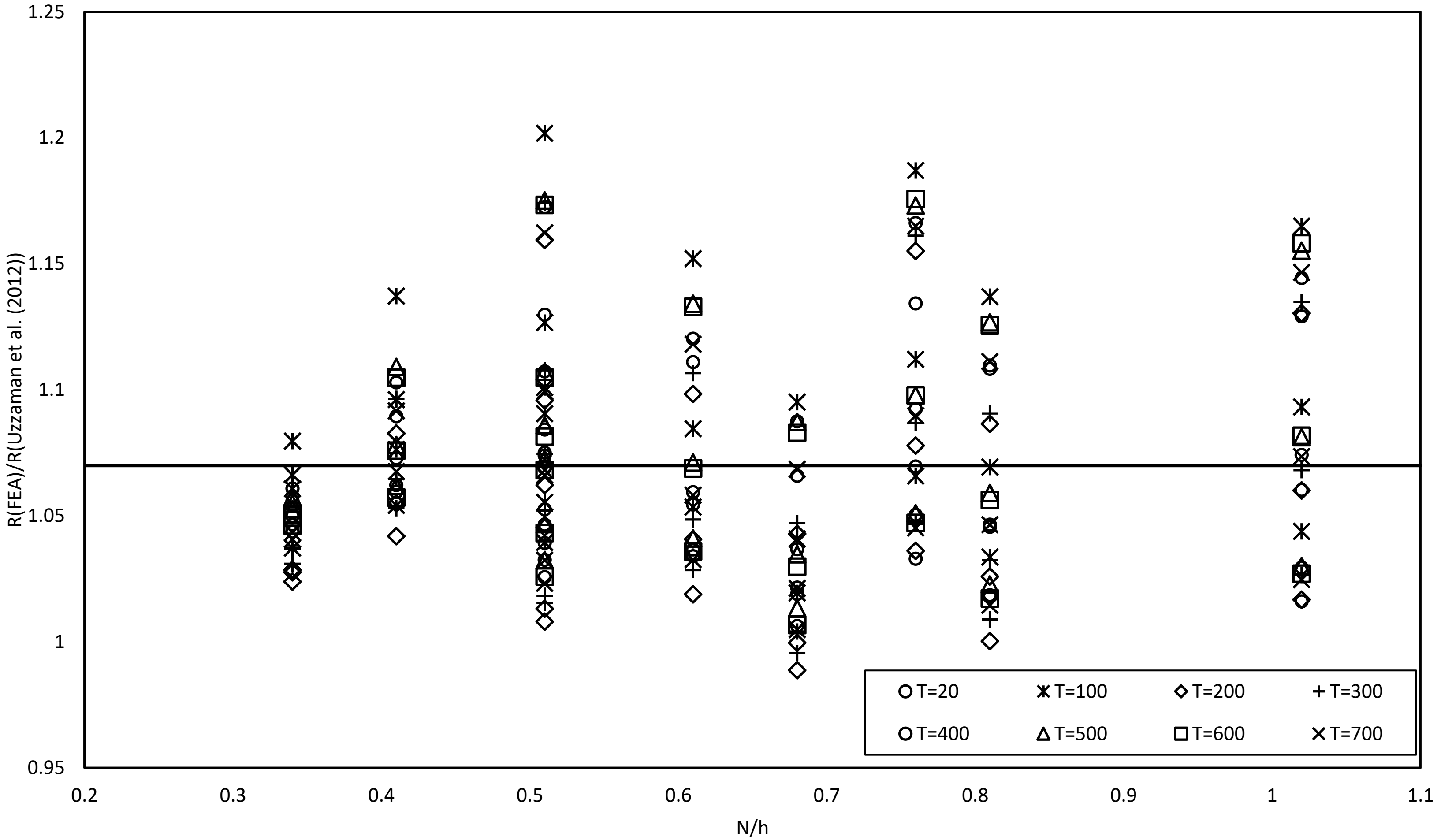

(b)

Figure7 Strength reduction factor comparison with centred circular web holes: a) R(FEA)/R$_{\text{Uzzaman et al. [26]}}$ vs a/h ratio, b) R(FEA)/R$_{\text{Uzzaman et al. [26]}}$ vs N/h ratio

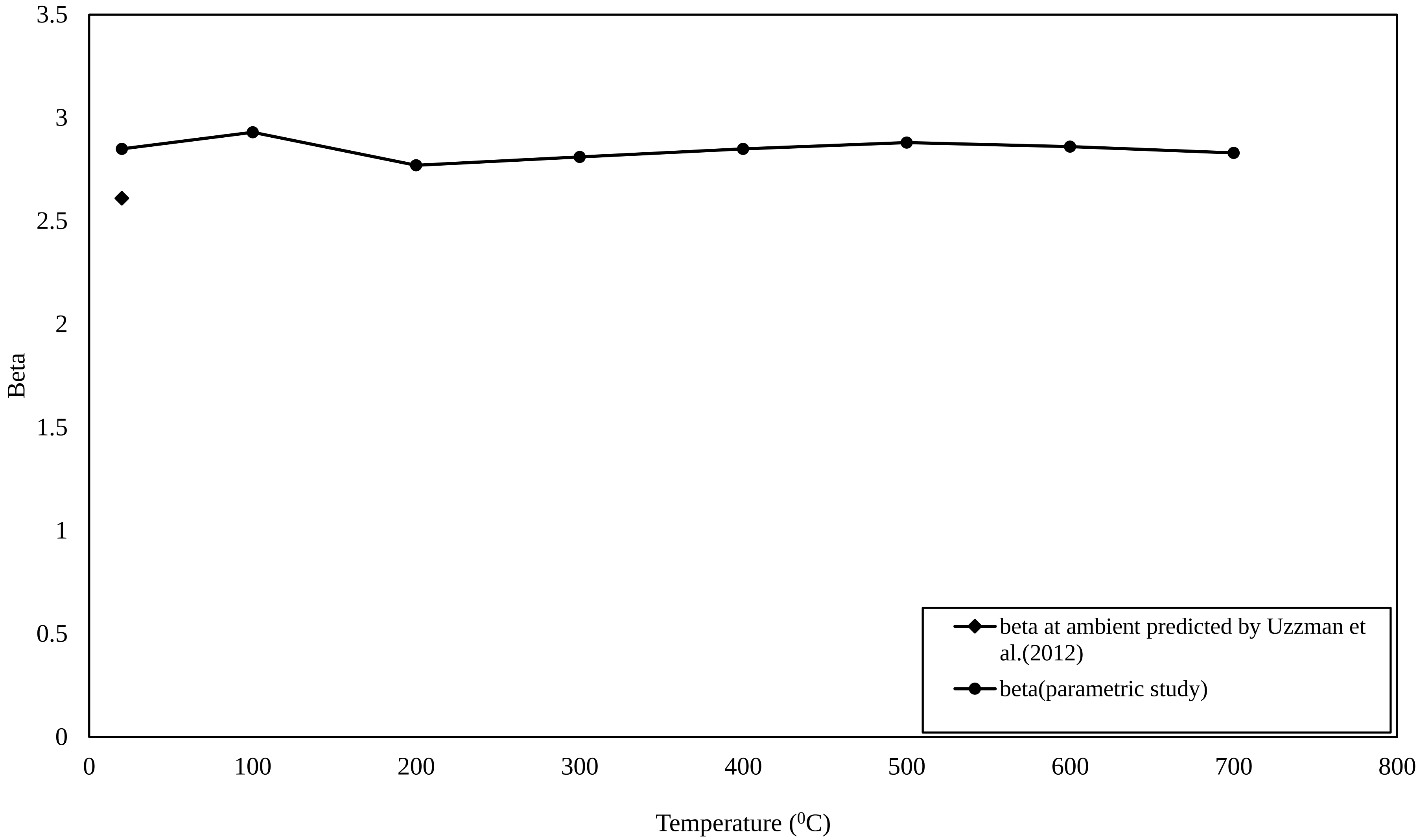

Figure8 Comparison of beta value obtained by parametric study and beta at ambient temperature presented by Uzzaman et al. [26]